Supporting Information

Promoted surface reconstruction of amorphous nickel boride electrocatalysts by boron dissolution for boosting oxygen evolution reaction

Yunzhu Du[1], Xiyu He[1], Cheng Yan[1], Qiaodan Hu[2], Junliang Zhang[1,*] and Fan Yang[1,*]

[1] Institute of Fuel Cells, School of Mechanical Engineering, Shanghai Jiao Tong University, 800 Dongchuan Road, Minhang District, Shanghai, 200240, China

[2] School of Materials Science & Engineering, Shanghai Jiao Tong University, 800 Dongchuan Road, Minhang District, Shanghai, 200240, China

*Corresponding authors.

junliang.zhang@sjtu.edu.cn (J. Zhang); fanyang_0123@sjtu.edu.cn (F. Yang)

The following additional results are provided in the sequence of their first citation in the main text.

1. ICP analysis on the synthesized NiB powder

Composition of the synthesized NiB powder was determined by ICP. Three independent batches of powder synthesized by identical procedures were measured to evaluate the compositional error from synthesis. The results are listed in Table S1. Based on the weight percentage of Ni and B, the atomic ratio between Ni and B is ~ 2.5. Thus, the powder was named as $Ni_{2.5}B$ for convenience.

Table S1 Composition of the synthesized NiB powder detected by ICP. Error bars are from three independent batches of powder.

Element	Content (wt. %)
Ni	84.10 ± 5.30
B	6.32 ± 0.38
O	Balance

2. Electrical conductivity of the synthesized NiB

The electrical conductivity of the synthesized NiB was evaluated using a four-probe resistivity tester (HPS2662, HELPASS Electronic Technologies Inc.). Prior to measurement, the NiB powder was compacted into a tablet with a diameter of 13 mm and a thickness of 0.44 mm under a uniaxial pressure of 200 MPa. The room-temperature resistivity of the compacted NiB tablet is 32.0 Ω·m, corresponding to an apparent electrical conductivity of 312.5 $S \cdot m^{-1}$. Such value is comparable to that of conductive carbon, for example, XC-72 (172 S/m [1]), thus the synthesized NiB catalyst can be considered sufficiently conductive.

3. Electrochemical double layer capacitance

The double layer capacitance (C_{dl}) before and after 10-hour chronopotentiometry test at a constant current density of 10 $mA \cdot cm^{-2}$ was obtained through cyclic voltammetry (CV) at different scan rates in a non-Faraday region, as shown in Fig.S1.

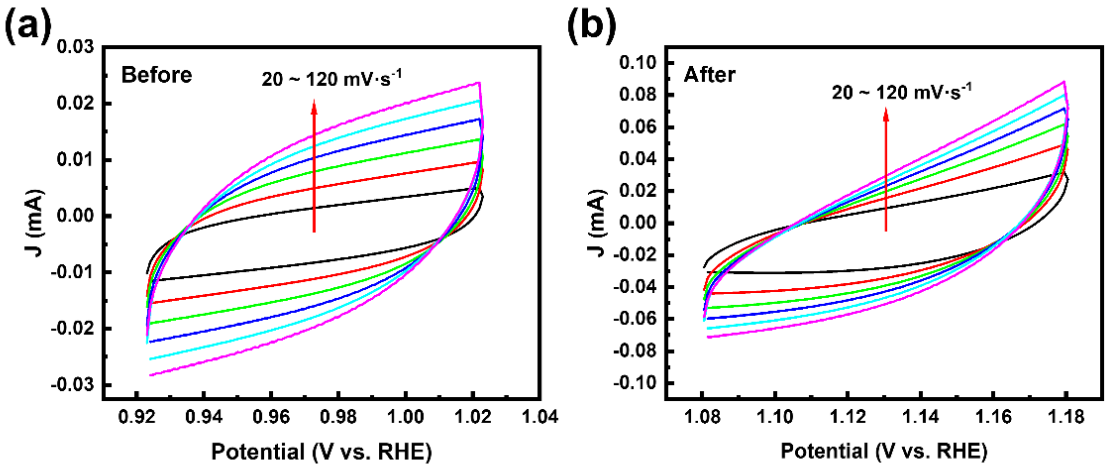

Figure S1 Cyclic voltammograms of nickel boride (a) before and (b) after 10-hour chronopotentiometry.

4. Comparison of the OER activity with literature data

The OER activity of the $Ni_{2.5}B$ catalyst was compared with those of other transition-metal borides reported by literature, as listed in Table S2. When the reaction reaches a stable state, i.e., the surface reconstruction reaches equilibrium, the overpotential at 10 mA/cm^2 of the $Ni_{2.5}B$ catalyst in this work, especially when loaded on the conductive Ni foam substrate, is comparable to (if not superior to) many multi-cation TMBs.

Table S2 Comparison of OER performance with other reported transition-metal borides catalysts in 1.0 M KOH electrolyte. η_{10} represents the overpotential at 10 mA/cm^2.

Catalyst	η_{10} (mV)	Tafel slope (mV/dec)	Reference
$Ni_{2.5}B$@CFP	343	63.7	This work
$Ni_{2.5}B$@Ni foam	279	-	
$FeCoB_2$	295	84	[2]
Co-Mn-Ni-P-B-O	360	62	[3]
Co-Fe-B	280	38.9	[4]
CoB	400	65.9	
FeB	450	58.4	
CoFeNiMnZnB	261	56.8	[5]
CoFeNiMnB	274	69.3	
A-CoB/f -CNF	350	173	[6]
Co-B thin film	280	-	[7]
Co_2−Fe−B	298	62.6	[8]
NixB nanosheets	380	89	[9]
Ni-Bi@NB	364	65	[10]
Partially crystalline Ni-Bi@NB	302	52	
Ni_3B	409	-	[11]
Co_2B-500-NG	360	45	
Co_2B-500	380	-	

5. Additional CV and LSV results for $Ni_{2.5}B$

The OER performance of nickel boride electrode was also studied by 1000 cycles of CV scans at 50 $mV \cdot s^{-1}$, as shown in Fig.S2. The anodic current density increases with increasing CV cycles and then reaches a stable state, as indicated by the red arrow in the figure. LSV curves before and after 1000 CV cycles are presented in Fig.S3. Significant change on the polarization curve can be observed with reduced η_{10} and splitting of the Ni^{2+}/Ni^{3+} oxidation peak.

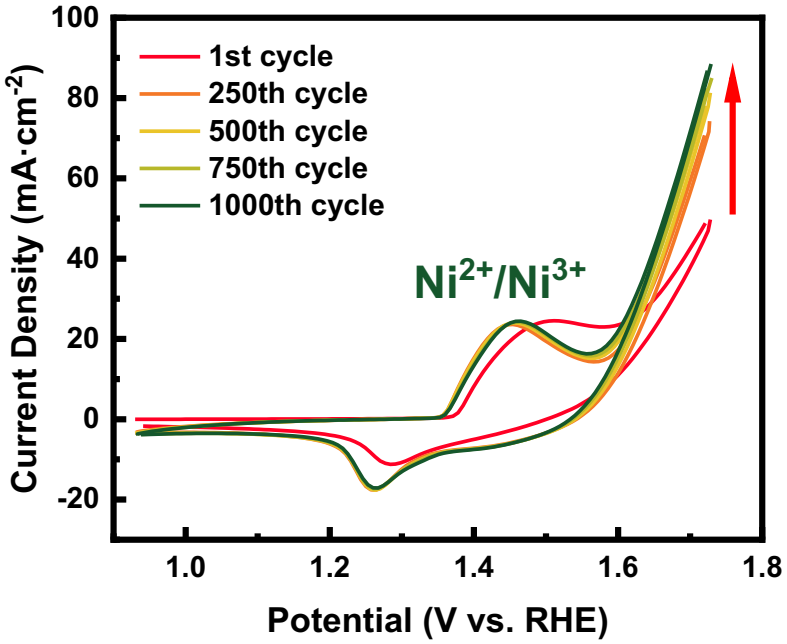

Figure S2 1000 cycles of cyclic voltammogram for nickel boride.

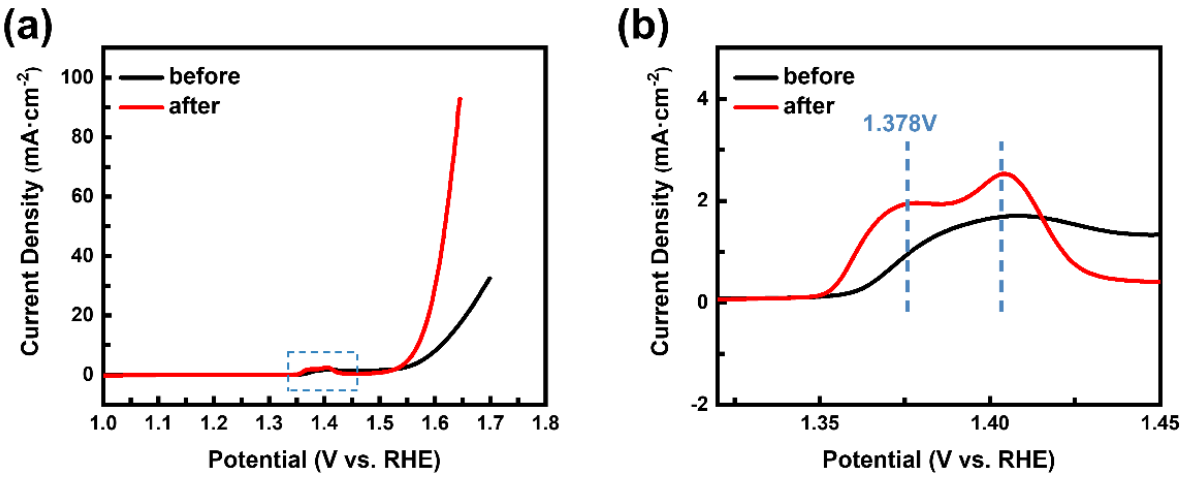

Figure S3 (a) LSV curves of $Ni_{2.5}B$ before and after 1000 cycles; (b) An expanded view of the dashed rectangular region in (a).

6. SEM images of the NiB electrode before and after chronopotentiometry

SEM images of the $Ni_{2.5}B$ catalyst before and after OER both show irregular, agglomerated flake-like microstructures, as shown in Fig.S4. No significant change in the particle morphology can be observed after OER.

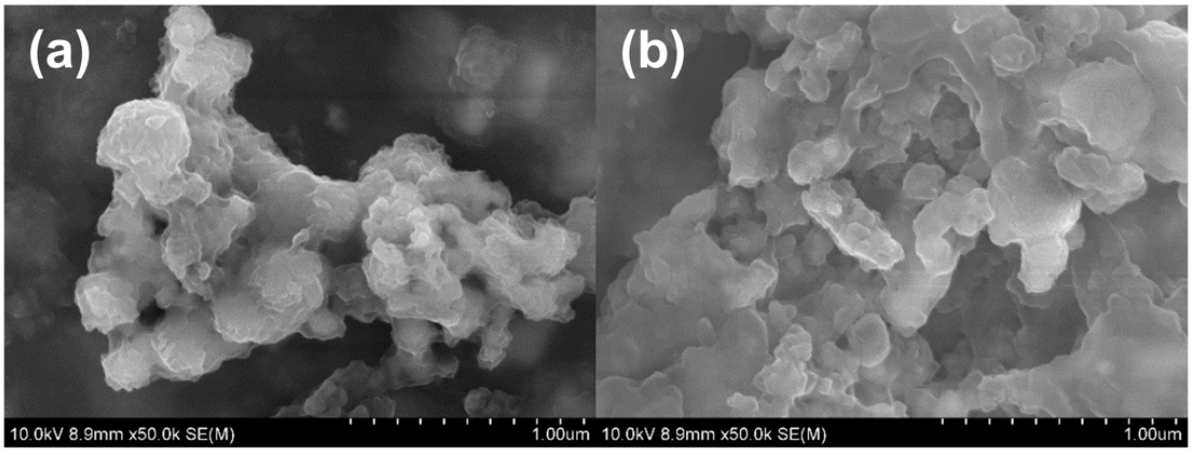

Figure S4 SEM images of nickel boride electrode (a) before and (b) after 10-hour chronopotentiometry.

7. TEM and EDS mapping results of nickel boride after chronopotentiometry

The particle morphology and elemental distribution of the $Ni_{2.5}B$ catalyst after OER is further investigated by TEM, as shown in Fig.S5. $Ni_{2.5}B$ after OER displays irregular-shaped nano particles (Fig.S5a), which is similar to that before OER (Fig.1d) . HRTEM image (Fig.S5b) shows some fuzzy lattice fringes, whereas the inserted SAED pattern reveals that the main structure of $Ni_{2.5}B$ after chronopotentiometry remains amorphous. EDS elemental mapping exhibits a uniform distribution of nickel, boron and oxygen.

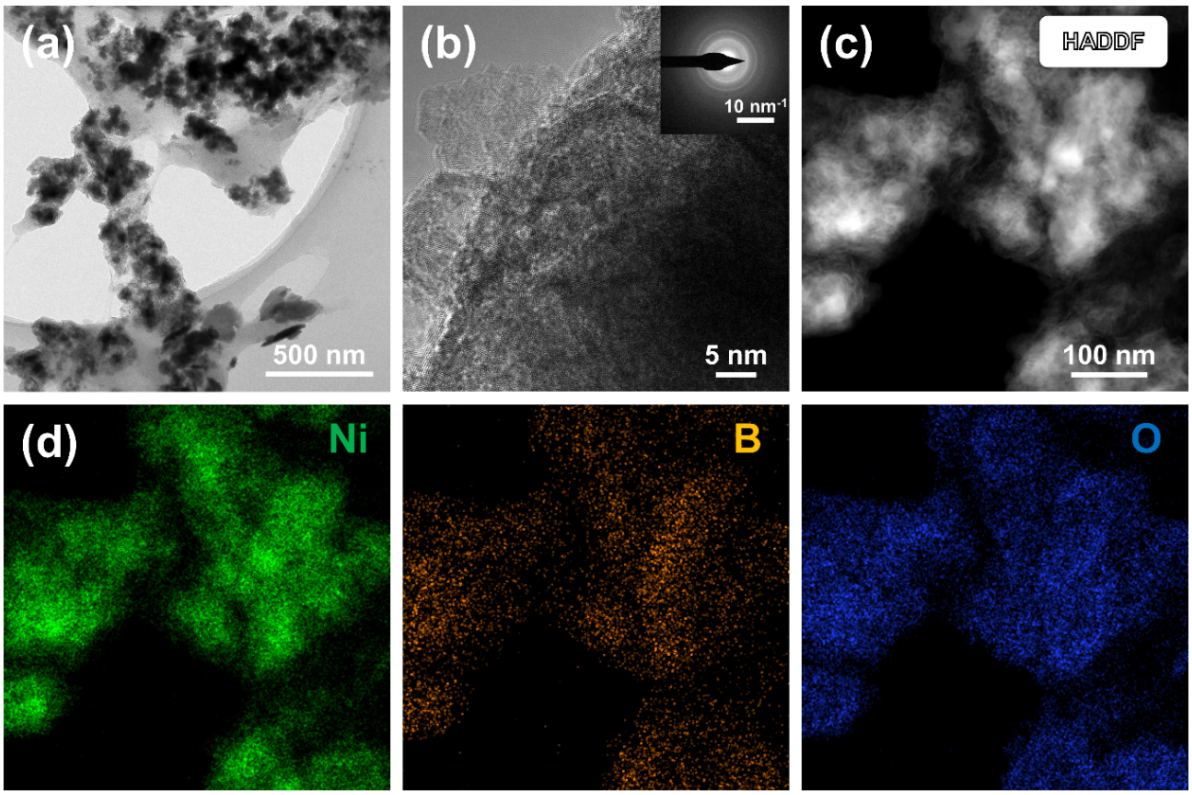

Figure S5 (a) TEM image; (b) HRTEM image, the inset image is the SAED pattern; (c) HADDF-STEM image and (d) EDS mapping images of Ni, B, and O after chronopotentiometry.

8. Designed boron dissolution experiments

The dissolution of boron from nickel boride electrode into the electrolyte during OER was monitored. The prepared CFP working electrode was tested by chronopotentiometry at a constant current density of 10 $mA \cdot cm^{-2}$ for 10 hours. The electrolyte was 100 ml 1.0 M KOH solution and was continuously stirred at 800 rpm. After each 2-hour chronopotentiometry test, LSV curves were recorded at a scan rate of 1 $mV \cdot s^{-1}$, and 2.0 ml electrolyte solution was extracted for ICP-MS detection.

The 10-hour chronopotentiometry curve of nickel boride at 10 $mA \cdot cm^{-2}$ with an interval of 2 hours is shown in Fig.S6. EIS performed at 1.5 V vs. RHE after each interval is presented in Fig.S7.

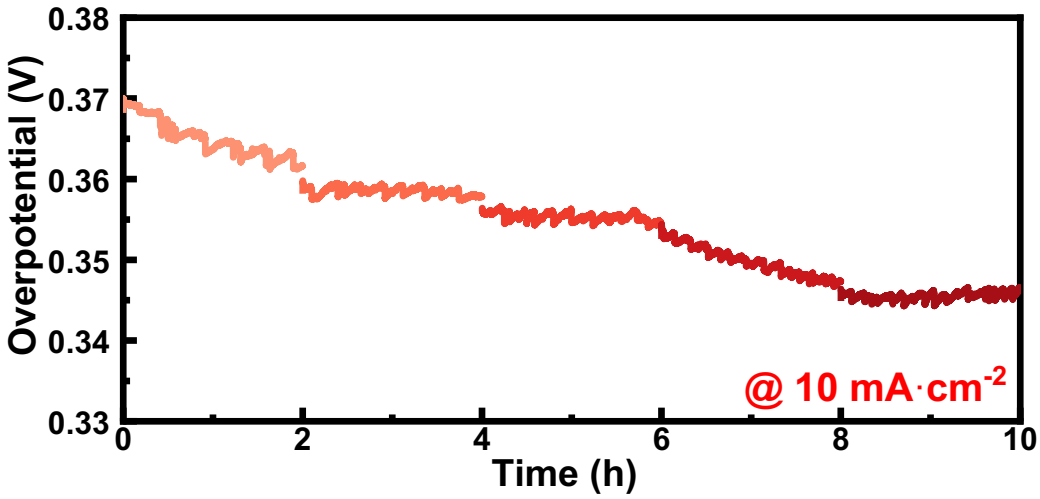

Figure S6 10-hour chronopotentiometry curve of nickel boride at 10 mA·cm^{-2} with an interval of 2 hours.

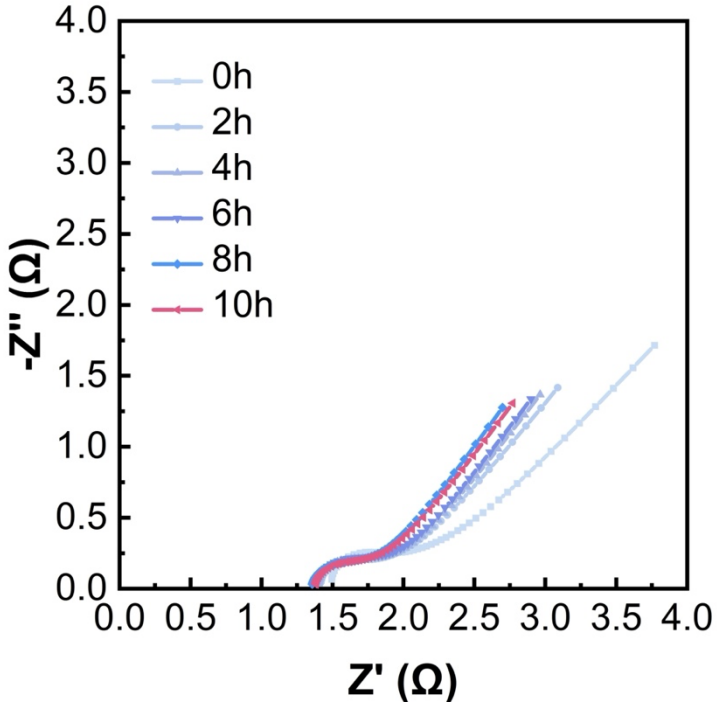

Figure S7 Nyquist plots at 1.5 V vs. RHE after each 2-hour chronopotentiometry test.

9. OER performance in the 1.0 M KOH solution added 0.1 M BO_2^-.

Chronopotentiometry curve of nickel boride at 10 mA·cm^{-2} in the 1.0 M KOH + 0.1 M BO_2^- electrolyte is shown in Fig.S8. The potential shows a small drop from 1.589 V (vs. RHE) to 1.575 V (vs. RHE) in the initial two hours and then remains stable, which is similar to the

phenomenon observed in 1.0 M KOH (Fig.2a in the main text). With the presence of BO_2^-, the initial η_{10} is reduced from 373 mV to 359 mV.

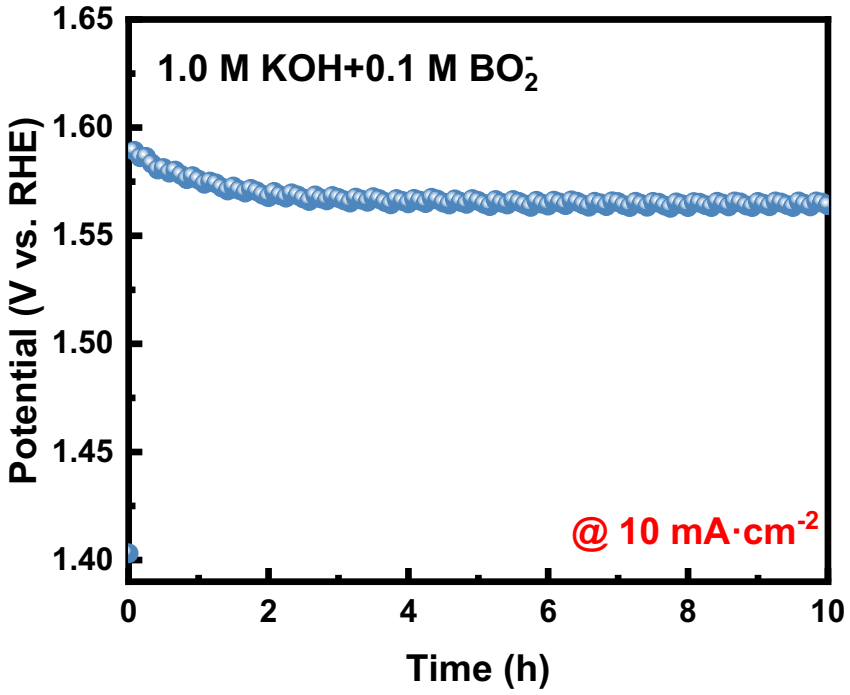

Figure S8 Chronopotentiometry curve of nickel boride at 10 mA·cm^{-2} in the 1.0 M KOH + 0.1 M BO_2^- electrolyte.

10. The calculated OER pathway on β-NiOOH by DFT

The four-step OER pathway on β-NiOOH is shown in Fig.S9.

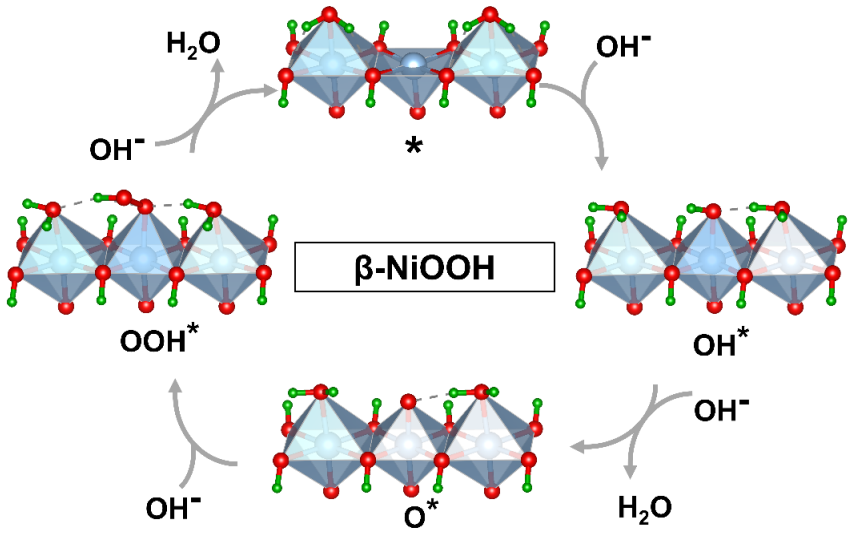

Figure S9 The four-step OER pathway on β-NiOOH.

11. Reference

[1] W. Zhang, G. Xu, R. Liu, J. Chen, X. Li, Y. Zhang and Y. Zhang, Novel MOFs@XC-72-Nafion nanohybrid modified glassy carbon electrode for the sensitive determination of melamine, Electrochimica Acta, 211 (2016) 689-696.

[2] X. Zou, W. Zhang, X. Zhou, K. Song, X. Ge and W. Zheng, The surface of metal boride tinted by oxygen evolution reaction for enhanced water electrolysis, Journal of Energy Chemistry, 72 (2022) 509-515.

[3] G. Lee and J. Kim, Effective tri-metal and dual-doped catalyst for oxygen evolution reaction: Amorphous Co-Mn-Ni-P-B-O nanoparticles, Applied Surface Science, 591 (2022) 153171.

[4] C. Qiang, L. Zhang, H. He, Y. Liu, Y. Zhao, T. sheng, S. Liu, X. Wu and Z. Fang, Efficient electrocatalytic water splitting by bimetallic cobalt iron boride nanoparticles with controlled electronic structure, Journal of Colloid and Interface Science, 604 (2021) 650-659.

[5] X. Wang, Y. Zuo, S. Horta, R. He, L. Yang, A. O. Moghaddam, M. Ibáñez, X. Qi and A. Cabot, CoFeNiMnZnB as a high-entropy metal boride to boost the oxygen evolution reaction, ACS Applied Materials & Interfaces, 14 (2022) 48212-48219.

[6] R. Sukanya and S. Chen, Amorphous cobalt boride nanosheets anchored surface-functionalized carbon nanofiber: An bifunctional and efficient catalyst for electrochemical sensing and oxygen evolution reaction, Journal of Colloid and Interface Science, 580 (2020) 318-331.

[7] S. Gupta, H. Jadhav, S. Sinha, A. Miotello, M. K. Patel, A. Sarkar and N. Patel, Cobalt-boride nanostructured thin films with high performance and stability for alkaline water oxidation, ACS Sustainable Chemistry & Engineering, 7 (2019) 16651-16658.

[8] H. Chen, S. Ouyang, M. Zhao, Y. Li and J. Ye, Synergistic activity of Co and Fe in amorphous Co_x-Fe-B catalyst for efficient oxygen evolution raction, ACS Applied Materials & Interfaces, 9 (2017) 40333-40343.

[9] J. Masa, I. Sinev, H. Mistry, E. Ventosa, M. de la Mata, J. Arbiol, M. Muhler, B. R. Cuenya and W. Schuhmann, Ultrathin High Surface Area Nickel Boride (Ni_xB) Nanosheets as Highly Efficient Electrocatalyst for Oxygen Evolution, Advanced Energy Materials, 7 (2017) 1700381.

[10] W. Jiang, S. Niu, T. Tang, Q. Zhang, X. Liu, Y. Zhang, Y. Chen, J. Li, L. Gu, L. Wan and J. Hu, Angewandte Chemie International Edition, 56 (2017) 6572-6577.

[11] J. Masa, P. Weide, D. Peeters, I. Sinev, W. Xia, Z. Sun, C. Somsen, M. Muhler and W. Schuhmann, Nonprecious catalyst for electrochemical water splitting: Oxygen and

hydrogen evolution, Advanced Energy Materials, 6 (2016) 1502313.